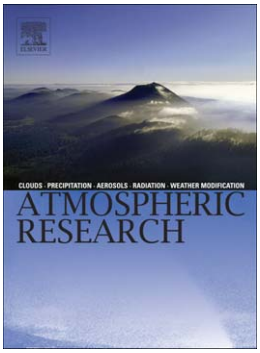

A study of the nocturnal flows generated in the north side of the Pyrenees

Maria A. Jiménez, Joan Cuxart

PII: S0169-8095(14)00192-6
DOI: doi: 10.1016/j.atmosres.2014.04.010
Reference: ATMOS 3147

To appear in: *Atmospheric Research*

Received date: 26 February 2014
Revised date: 11 April 2014
Accepted date: 21 April 2014

Please cite this article as: Jiménez, Maria A., Cuxart, Joan, A study of the nocturnal flows generated in the north side of the Pyrenees, *Atmospheric Research* (2014), doi: 10.1016/j.atmosres.2014.04.010

A study of the nocturnal flows generated in the north side of the Pyrenees

Maria A. Jiménez[a,*], Joan Cuxart[b]

[a] *Department of Global Change Research, Institut Mediterrani d'Estudis Avançats (UIB-CSIC), Esporles, Illes Balears, Spain*
[b] *Grup de Meteorologia, Departament de Física, Universitat de les Illes Balears, Palma de Mallorca, Illes Balears, Spain*

Abstract

During night-time, with clear-skies and weak-synoptic pressure gradients, the organization of the flow at lower levels is mainly controlled by the local effects, such as terrain or surface heterogeneities. This is the case of the thermal differences between the air adjacent to the slopes and over the nearby plains that generate downslope winds. The foothills of the north Pyrenees are selected to study the temporal and spatial scales of the downslope winds through a high-resolution mesoscale simulation. From the analysis of the model outputs and the observations, it is found that the organization of the flow at lower levels can be separated in three well-defined regions. At the mountain slopes, downslope winds appear close to the surface whereas down-valley winds form later, after the accumulation of air in the bottom of the valleys due to the downslope winds. At the foothills, the turning of the wind (from upslope to downslope) starts before sunset but it depends on the distance to the Pyrenees, the closer the earlier. Finally, at the Garonne river plain down-river winds are formed at the end of the night, after the accumulation of the downslope winds from the Pyrenees and the Massif Central. Furthermore, the physical mechanisms that take place while the downslope winds travel from the mountain to the plain regions are analysed.

*Corresponding author: Maria A. Jiménez. Department of Global Change Research, Institut Mediterrani d'Estudis Avançats (UIB-CSIC), Miquel Marquès 21, 07190-Esporles, Mallorca (Illes Balears) Spain. Telephone: +34 971611868.

Email addresses: majimenez@imedea.uib-csic.es (Maria A. Jiménez), joan.cuxart@uib.cat (Joan Cuxart)

Keywords: downslope winds, mesoscale modelling, mountain-plain winds, nocturnal boundary layer

1. Introduction

During night-time and under weak-synoptic pressure gradients, thermally-driven flows are developed over complex topography due to horizontal temperature differences (Whiteman, 2000). Downslope winds are produced by buoyant forces induced by the temperature difference between the air adjacent to the slope and the ambient air outside the slope whereas down-valley winds can be related to the thermal gradient along the valley axis. At a larger scale, the temperature difference between the air in a mountain massif and the air over the surrounding plains generates mountain-plain winds.

Zhong and Whiteman (2008), through mesoscale modelling and observations in the Salt Lake Valley, found that winds at the slopes inside the valley were weaker than downslope winds outside the valley. Stronger winds were found on the gentle slopes than on the steep slopes, similar to the analysis of Cuxart et al. (2012) in the Ebro basin, whose dimensions are larger than the Salt Lake Valley. From the temperature and momentum budget analysis, Zhong and Whiteman (2008) pointed out that the observed downslope winds were produced by the local cooling of the slope surface. A similar pattern was found by Cuxart et al. (2007) in a quasi-bidimensional gentle slope in the Mallorca Island and by Martínez and Cuxart (2009) in a larger and more heterogeneous slope in the Duero river basin. From tethered balloon soundings, Haiden and Whiteman (2005) showed that the local topography along a gentle slope was the responsible for the along-slope flow variations. Slope winds may interact with lake breezes (Laiti et al., 2013) or with sea breezes (Cros et al. (2004); Bastin et al. (2005)) changing their intensity or the distances they reach.

The area north to the central Pyrenees, in the Garonne basin, is chosen to analyse the different types of downslope and down-valley winds generated within because it is a good example of steep mountain range adjacent to a wide plain area. This basin is limited by the Pyrenees at the south and the Massif Central at the east, and the river flows from south-east to north-west to the Atlantic Ocean (Fig. 1). The influence of the Pyrenees on the atmospheric synoptic flow was analysed in the Pyrenees experiment field campaign (PYREX, (Bougeault et al., 1990)). The dense network of observations at the north and south sides of the Pyrenees during fall 1990 showed

that higher and lower pressures at north and south sides of the Pyrenees, respectively, were the responsible of the formation of the three well-known regional wind systems in the area (Bougeault et al., 1997): Autan (south-eastern wind close to Toulouse), Tramontane (north and north-western wind in the Gulf of Lion, Campins et al. (1995)) and Cierzo (north-western wind in the Ebro river basin, Masson and Bougeault (1996)), see locations in Fig. 1. Recently, the Boundary Layer Late Afternoon and Sunset Turbulence (BLLAST) experimental field campaign has been made in Lannemezan (labelled as LZ in Fig. 1), at the foothills of the Pyrenees, during June and July 2011. The aim of this project is to have more and better observations of the late afternoon transition and to further explore the mechanisms that control it. Observations are currently being analysed (Lothon et al., 2010).

The current work is devoted to study the organization of the flow at lower levels under night-time conditions in the northern Pyrenees through the inspection of a high-resolution mesoscale simulation. The main objective is to analyse the relevant factors in the generation of downslope winds and characterise their temporal and spatial scales. The simulated conditions and the model setup are explained in section 2. In section 3 the organization of the flow is analysed and section 4 is devoted to a deeper study of the downslope winds in the foothills region. Finally, the conclusions are given in section 5.

2. Model setup and description of the simulated conditions

The mesoscale model MesoNH (Lafore et al., 1998) is run with a setup already used in previous studies. For instance, the organization of the flow during the night-time in the Island of Mallorca made by Cuxart et al. (2007), in the Duero river basin as described in Martínez et al. (2010) or, more recently, in a fog case event in the Ebro river basin (Cuxart and Jiménez, 2012). For all the regions studied, the model provides results that compare well to the available observations. A brief description of the model choices is given in Table 1. The horizontal resolution is 2 km $\times$ 2 km and covers the Garonne river basin, including the Pyrenees and the west part of the Massif Central. The vertical resolution is fine close to the surface (3 m) and becomes coarser as height increases in order to have a better characterization of the physical processes that take place at lower levels, as it was pointed out by Jiménez et al. (2008).

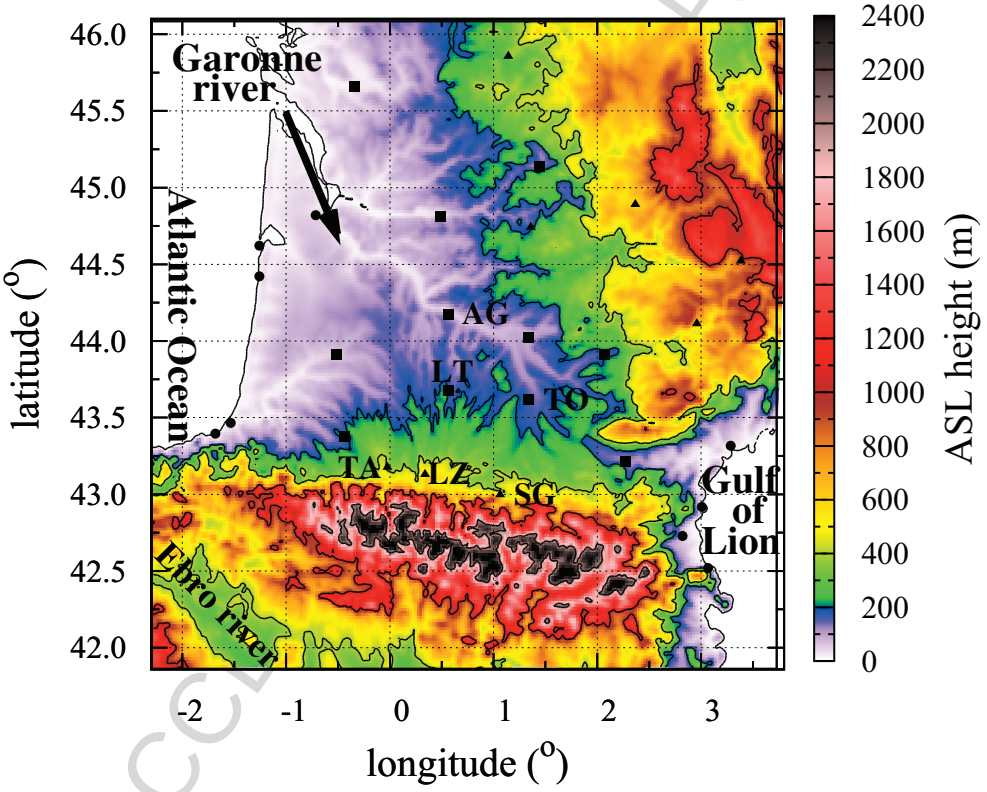

Figure 1: Simulation domain which covers the Garonne river basin with the Pyrenees at the south and the Massif Central at the east. Topography lines at 200, 400, 1000 and 2000 m (above sea level, ASL) are labelled and in dots there are the locations of the available surface weather stations (in circles the stations at the coast, in squares those at the plain and in white triangles at the foothills). Some of the locations are labelled (SG: Saint Girons, TA: Tarbes and LZ: Lannemezan in the slopes and TO: Toulouse, AG: Agen and LT: Lamonthe in the plain).

Table 1: Summary of the setup of the run made with the MesoNH model (Lafore et al., 1998).

Domain	200 ×300 gridpoints
Horizontal Resolution	2 × 2 km

Vertical resolution (following-terrain coordinates)	near the ground: $\Delta z = 3$ m;
	at z = 500 m: $\Delta z = 7$ m;
	top of the domain at 9270 m with $\Delta z = 600$ m

Equation system	Durran (1989)
Initial and lateral boundary conditions	Analysis from the ECMWF every 6 hours
Radiation scheme	Morcrette (1990) Longwave: Mlawer et al. (1997) Shortwave: Fouquart and Bonnel (1980)
Advection Scheme	Flux corrected second order centered
Turbulence Scheme	TKE scheme: Cuxart et al. (2000) mixing length: Bougeault and Lacarrère (1989)
Surface Scheme	Soil and vegetation: ISBA (Noilhan and Planton, 1989) Sea and inland waters: Belamari (2005) Urban and artificial areas: Masson (2000) Land use: ECOCLIMAP (Masson et al., 2003)

2.1. The case studied

A case with a weak synoptic pressure gradient and clear-skies in the area of interest is chosen. The simulated period goes from 30th June 2010 at 0600 UTC until 1st July 2010 at 1000 UTC (local time is equal to UTC time for this area) to allow the model to develop the nocturnal circulations after the diurnal spin-up. The run is initialised using an analysis of the European Centre for Medium-Range Weather Forecasts (ECMWF) and the lateral boundary conditions are refreshed every 6 hours. The domain is wide enough to cover the Pyrenees mountain range and the foothills region, to have a proper representation of the downslope winds and avoid problems with the lateral boundary conditions, as it is suggested by Warner et al. (1997).

The synoptic wind in the area of interest is weak (the estimated geostrophic wind is around 1 m s^{-1}) from north at the beginning of the run later turning to south-west due to a low pressure system located in the western side of England. Therefore, the turbulence, the radiation and the surface schemes play a central role in the modelled evolution of the flow.

Observations in Lannemezan (at the foothills of the Pyrenees, labelled as LZ in Fig. 1) during the period 2001-2009 show that about 50 % of the days have slope winds (Barneoud et al., 2010). In good correspondence with the local topography of the area, during the day the wind is from the northern sector (uphill) whereas it is from southern sector at night (downhill). The chosen period in this work is a representative case of the atmospheric conditions where slope winds are generated, according to Barneoud et al. (2010).

2.2. Observations

The data available to us from the French meteorological official network is not large. Besides, many of the stations are located at the coast, in very narrow valleys and/or in the peak of mountains (see dots in Fig. 1).

During the night 30th June - 1st July 2010, the wind speed at 10 m was weak (on average, less than 2 m s^{-1}) in most of the available surface stations in the basin. The 10 m - wind direction followed the local slopes, indicating that this factor was the main responsible for the organization of the flow at lower levels.

Observations from some selected automatic surface weather stations in the foothills coloured in yellow and green in Fig. 1 (Lannemezan, Saint Girons and Tarbes, labelled as LZ, ST and TA, respectively) and plain in

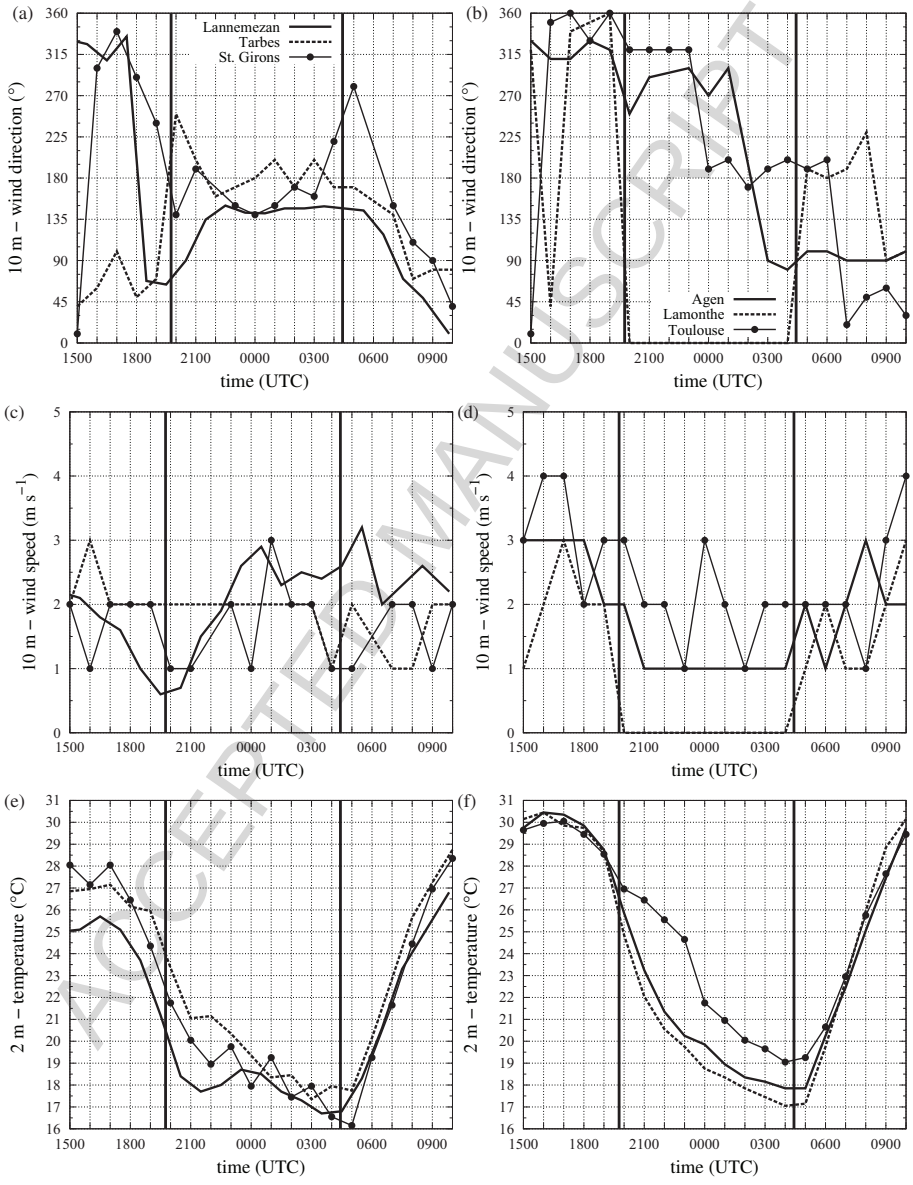

Figure 2: Observed time series at some selected surface stations at the foothills (left, Lannemezan, Saint Girons and Tarbes) and at the plain (right, Agen, Toulouse, Lamonthe). The locations are indicated in Fig. 1. (a) and (b) 10 m - wind speed (in m s^{-1}); (c) and (d) 10 m - wind direction (in °) and (e) and (f) 2 m - temperature (in °C). Time goes from 1500 UTC on 30th June 2010 to 1000 UTC of the next day. The black vertical lines indicate the sunset and sunrise hours.

blue in Fig. 1 (Agen, Toulouse and Lamonthe, labelled as AG, TO, LT, respectively) are shown in Fig. 2.

At the foothills and plain, during the central part of the day, the wind is from the north, corresponding to the uphill direction (Fig. 2a and 2b). At the foothills, the turning of the wind starts 2 hours before sunset and takes 4 hours to become south-east, a direction that will remain during the whole night (Fig. 2a). This turning is nearly simultaneous (the starting and the duration) in all the selected stations at the foothills since all of them are placed at about the same distance from the mountain range slopes. On the other hand, at the plain (Fig. 2b) the turning of the wind starts later, at midnight in Toulouse and 3 hours later in Agen, when the air that flows down from the Pyrenees reaches the area. However, in all locations at the plain the turning is completed faster than at the foothills. Since Agen is farther from the Pyrenees than Toulouse the turning of the wind starts later than in Toulouse. Nothing can be said about Lamonthe where observations indicate calm winds from sunset to sunrise.

The wind speed at the foothills is close to calm at sunset (1945 UTC) and it increases afterwards, with values lower than those during the daytime (Fig. 2c) but this pattern is not seen as clearly as at the plain (Fig. 2d). At the foothills, the cooling rate is larger in the evening (7 K/4 h, Fig. 2e), when the winds are less intense and the net radiation rapidly decreases, than after midnight (2 K/5 h), when the downslope winds are established. On the other hand, the cooling rate is constant in Lamonthe and Agen (placed at the plain, Fig. 2f) during the whole night (9 K/5 h in the evening and 2 K/4 h after midnight). Although Toulouse is also located at the plain, at 0000 UTC the wind suddenly changes from upslope to downslope directions meanwhile the wind speed increases and the 2m-temperature decreases 3 K/1 h. This might indicate that the downslope winds travelling from the mountain range to the plain are colder than the air at the foothills. This is further explored in section 4 through the model outputs.

Just after sunrise (0425 UTC) the temperature warms up fast (10 K/5 h at the foothills and 12 K/5 h at the plain). About 2.5 hours later (0600 UTC), at the foothills the wind veers to north (upslope direction) and the turning is delayed at the plain while the wind speed slightly decreases (Fig. 2c).

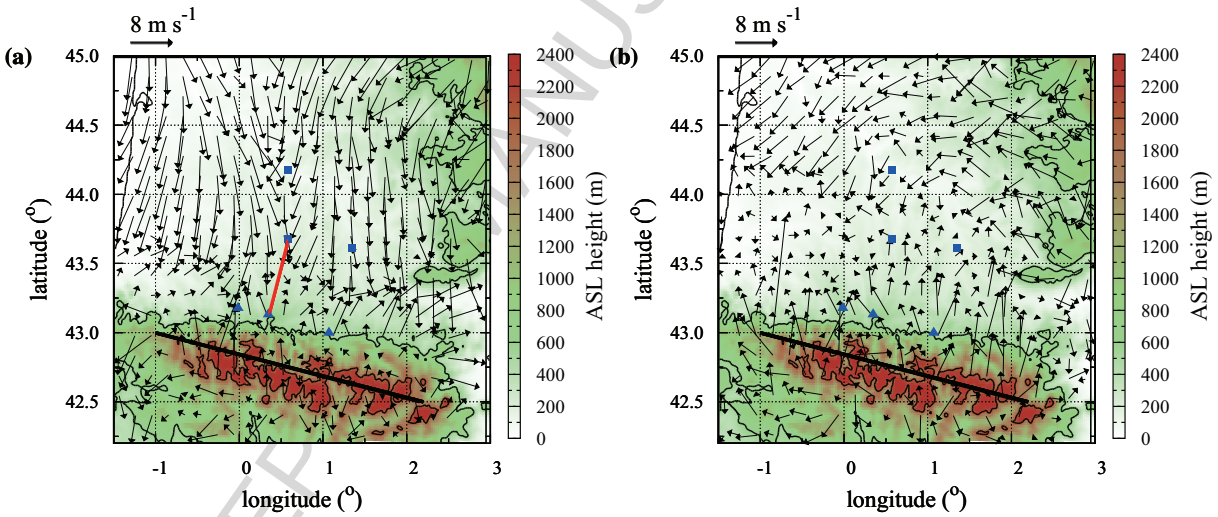

Figure 3: Wind vectors at 50 m AGL over the topography (in colours) at different instants: (a) 30th June at 2200 UTC and (b) 1st July at 0400. There is one arrow plotted every 8 gridpoints (16 km) and the length indicates the intensity of the wind (maximum intensity 8 m s^{-1}). The topography lines at 400, 600, 1000, 2000 and 2400 m ASL are also included. The vertical cross-section in Fig. 4 is indicated with a red line. The black line above the Pyrenees indicates the zero distance in Fig. 7 and 8. The surface stations in Fig. 2 are indicated with blue triangles (foothills) and squares (plain).

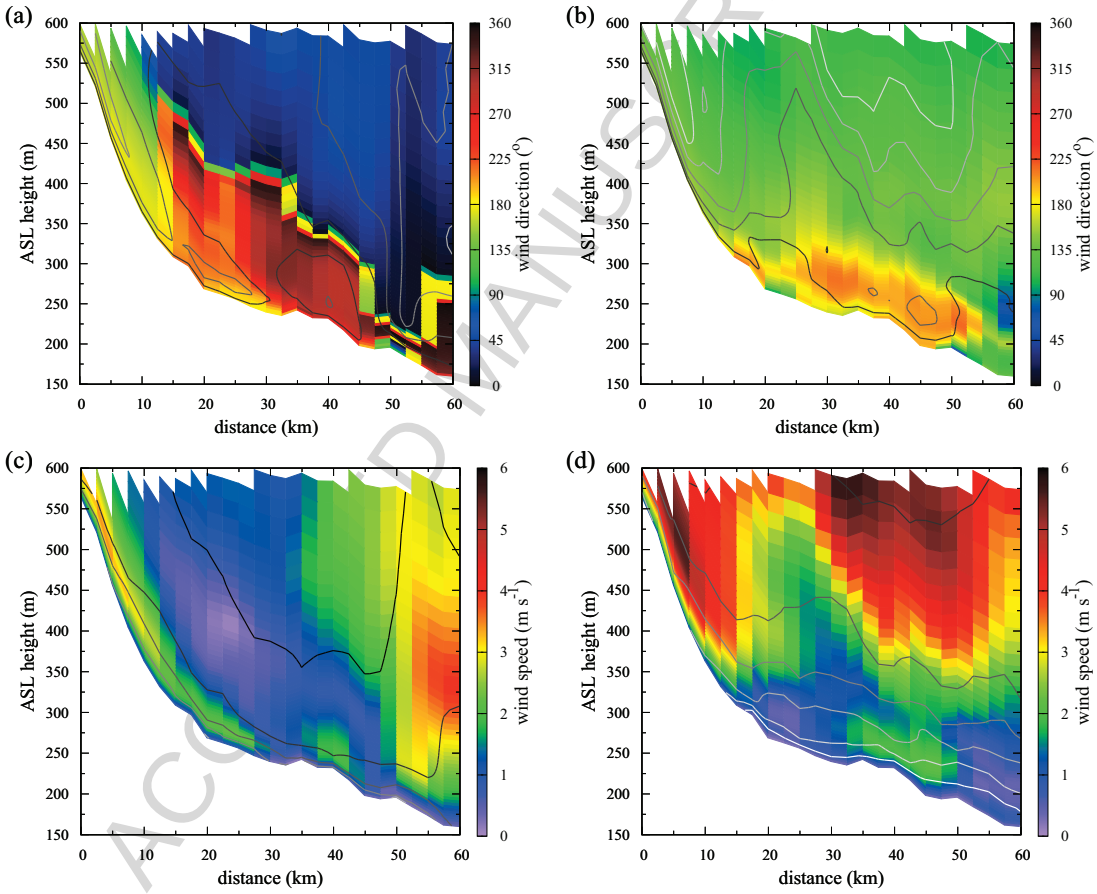

Figure 4: Vertical cross-sections over the foothills region (from Lannemezan to Lamonthe, indicated with a red line in Fig. 3a). (a) and (b) Wind direction (in colours) and wind speed (in lines every 1 m s^{-1}) at 2200 UTC and 0400 UTC, respectively. The same in (c) and (d) but for the wind speed (in colours) and the potential temperature (in lines every 1 K starting from 295 K in white and 301 K in black).

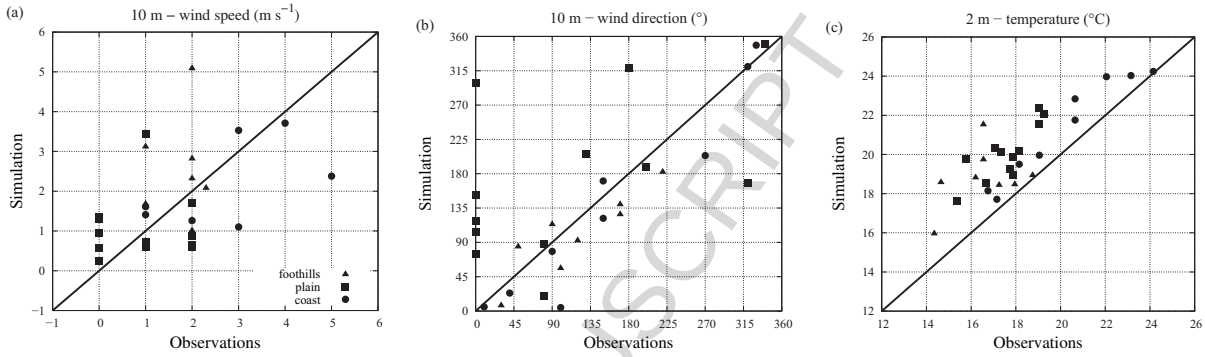

Figure 5: (a) Comparison of the observed and simulated 10 m - wind speed (in m s^{-1}) at 0400 UTC for the surface stations indicated in Fig. 1. Each symbol is related to the region where the surface station is located. The same in (b) and (c) for the 10 m - wind direction (in °) and 2 m - temperature (in °C), respectively. The diagonal shows the ratio 1:1.

3. Model results

To illustrate the modelled patterns at lower levels in the Garonne river basin, Fig. 3 shows the wind vectors at 50 m above the ground level (AGL) at 2200 UTC and 0400 UTC.

Before sunset, the synoptic wind has weakened and the local effects play the main role at lower levels, similarly to what is found in other locations that have been studied using a similar model setup (Cuxart et al. (2007); Martínez et al. (2010)). At 2200 UTC (Fig. 3a), the model shows that the predominant direction of the wind at lower levels is from south at the foothills of the Pyrenees, corresponding to the downslope wind direction. Fig. 3a clearly indicates that downslope winds are present at the foothills whereas at the plain the wind has still the diurnal direction (north), in agreement with the observations in Fig. 2. This is related to a low-pressure system placed in the western side of England that generated northerly winds in the Garonne river basin at the beginning of the simulation but it weakens as time advances. As night progresses, the air flows down to the middle Garonne from where the wind blows down-river to the Atlantic Ocean. The model results at 0400 UTC (Fig. 3b), agree with the observations and downslope winds are present at the plain and foothills.

To further evaluate the slope winds seen by the model, the vertical cross-sections of the temperature and wind fields from Lannemezan to Lamonthe (following the red line in Fig. 3a) are shown in Fig. 4 at 2200 UTC and

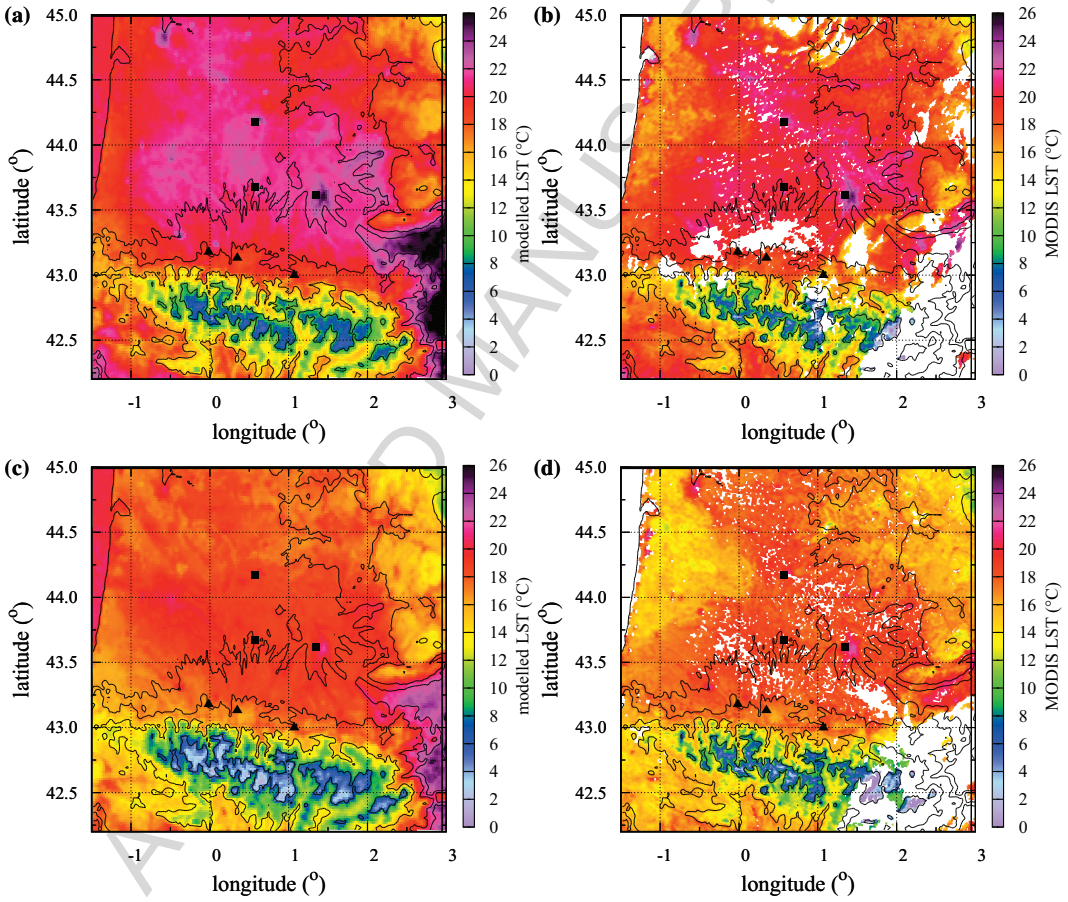

Figure 6: Land-Surface Temperature (LST, in °C) obtained from the model (left panel) and derived from MODIS (right panel) at two instants: (a) and (b) 30th June at 2200 UTC and (c) and (d) 1st July 0200 UTC. The topography lines at 400, 600, 1000, 2000 and 2400 m ASL are also included. The surface stations in Fig. 2 are indicated with black triangles (foothills) and squares (plain).

0400 UTC, corresponding to the early and mature phases of the slope winds, respectively. It is found that the downslope winds are initiated in the upper part of the foothills and as the night progresses they travel to the river, following the local slopes. Thus, at 2200 UTC the wind is from south in the upper part of the foothills whereas it is from north in the southern part (Fig. 4a). The maximum intensity of the downslope winds is located close to the surface (about 50 m AGL), at the top of the surface inversion (Fig. 4c), and with intensities of about 3-4 m s^{-1}.

At 0400 UTC, the wind is from south in the foothills and plain (Fig. 4b). However, downslope winds are more intense in the upper part of the foothills (Fig. 4d) than in the lower part where they are more elevated (about 100 m AGL). This is related to the presence of jets at the exit of the valleys, as it was found in Pamperin and Stilke (1985) from atmospheric soundings at the exit of the Inn valley (Austria). The model is able to reproduce these valley exit jets when the resolution is accurate enough to reproduce the topographical features of the valleys. However, the analysis of the valley exit jets is beyond the objectives of this work.

3.1. Verification

The verification of the model is made using the available surface observations in the Garonne river basin (see locations in Fig. 1). The modelled results agree with the available surface stations in the Garonne river basin as it is seen in Fig. 5. The 10 m wind speed and direction are well reproduced by the model although it overestimates the observed calm winds in some stations, mainly located in the plain, because the measured wind is close to the threshold value of the wind sensors. On the other hand, the model is not able to reproduce the nocturnal cooling at most of the stations located in the slope and plain areas (Fig. 5c). This is further explained at the end of this section.

According to Jiménez et al. (2008) the modelled surface temperatures can be compared to those derived from satellite images. Data from MODerate resolution Imaging Spectroradiometer (MODIS, Salomonson et al. (1989)) on board of the polar Aqua and Terra satellites (version 5 data Level 2) are used, covering the area of interest at an approximate nominal horizontal resolution of 1 km $\times$ 1 km (at nadir). During the studied period, there are two available MODIS Land-Surface Temperature (LST) fields: at 2200 UTC and 0200 and in Fig. 6 they are compared to those LST obtained from the

MesoNH model. The white areas in the MODIS images indicate the presence of high-clouds.

It is found that the model is able to reproduce the observed temperature patterns in the Garonne river basin. The model sees that the city of Toulouse is warmer than its surroundings, in agreement with the satellite observations. During the evening (at 2200 UTC, Fig. 6a and 6b), the model is able to reproduce the satellite-observed patterns the foothills but it has a warm bias up to 2 K in some areas at the plain.

At night (0200 UTC, Fig. 6c and 6d), the model is not able to reproduce the cold area in the west side of France, a forested area called *Parc naturel régional des Landes de Gascogne*. It is important to have in mind the two types of LST fields that are compared here. For this forest region, the MODIS LST corresponds to the temperature at the top of the tree whereas the modelled one corresponds to the temperature at the surface, below the trees. In night-time conditions, and in a dense forested area, the temperature difference between the surface and the top of the tree can be significantly large. This might explain the differences between the modelled and satellite-derived LST in the *Les Landes* region.

The comparison of the modelled and observed temperatures close to the surface indicates that, at the end of the night, the model is about 1-2 K warmer than the observations (Fig. 5c and 6) as it was pointed out by Jiménez et al. (2008) for a similar simulation over the Island of Mallorca or Martínez et al. (2010) in the Duero basin. They found that the chosen resolution of the topography and the representation of the surface characteristics in the model climatological database were the responsible of the warm bias between the simulated and observed 1.5 m - temperature fields. A similar warmer bias for the nocturnal temperatures was found by Seaman et al. (2012) through a mesoscale simulation over a more complex terrain region in Pennsylvania (USA) or by Edwards (2009) or Zhang et al. (2009) for climate simulations over the United States. On the other hand, under calm nights mixing is enhanced at lower levels in most of the turbulence schemes (as it is seen in the intercomparison exercise of Cuxart et al. (2006)) and, consequently, it does not allow enough surface cooling, independently of the chosen horizontal resolution, as it was pointed in Jiménez and Cuxart (2005).

The differences between the model results and the observations can be also related to the Monin-Obukhov similarity theory applied and lower levels that imposes a behaviour in the surface layer that might not correspond to the observed one.

4. The winds at the foothills and plain

4.1. Analysis of the southerly wind

To evaluate the spatial and temporal evolution of the downslope and down-valley winds on the foothills and plain of the Pyrenees, the modelled gridpoints of this region have been classified according to the wind direction at lower levels (up to 200 m AGL) for several instants from 1800 UTC to 1000 UTC of the next day. Fig. 7 shows the percentage of the grid points with a southerly wind (wind direction below 200 m AGL ranging between 120°-240°) along the black line in Fig. 3 and along an equally long line at a certain distance, perpendicular to it.

The averaged topography and the standard deviation for the whole line and for each distance is also included in the plot to have an estimation of the three main regions of interest. The largest mean heights and standard deviation values are in the mountain region (distances from 0 to 30 km in Fig. 7) and it mainly includes valleys between high mountain peaks in the Pyrenees. The lowest mean heights are found in the plain (distances larger than 100 km in Fig. 7). Between those regions, the foothills region is considered (from 30 km to 100 km in Fig. 7) where the mean height decreases with the distance.

Close to the sunset (Fig. 7, top), the percentage of points with southerly wind speed starts to be significant at the foothills of the Pyrenees and inside the valleys in the mountain region. It is related to the beginning of the local generation of downslope winds and the amount of points increases as the night advances.

From 2200 UTC to 0200 UTC (Fig. 7, middle) the distance from the Pyrenees where downslope winds are found increases progressively in time (about 40 km in 4 hours, with an averaged wind speed of 2.8 m s^{-1}) since the air flows down following the local topography to reach the middle Garonne river. Inside the valleys (the mountain region in Fig. 7), the number of points with down-valley winds increases, since the valley exit jets are formed. At the foothills, the percentage decreases with the averaged terrain elevation above the sea level and the maximum remains nearly constant (around 70 %), meanwhile at the plain region it is close to zero.

From 0200 UTC to 0600 UTC, the number of points with southerly wind starts to increase at the plain region. This can be related to down-river winds generated after the accumulation of air in the middle Garonne river

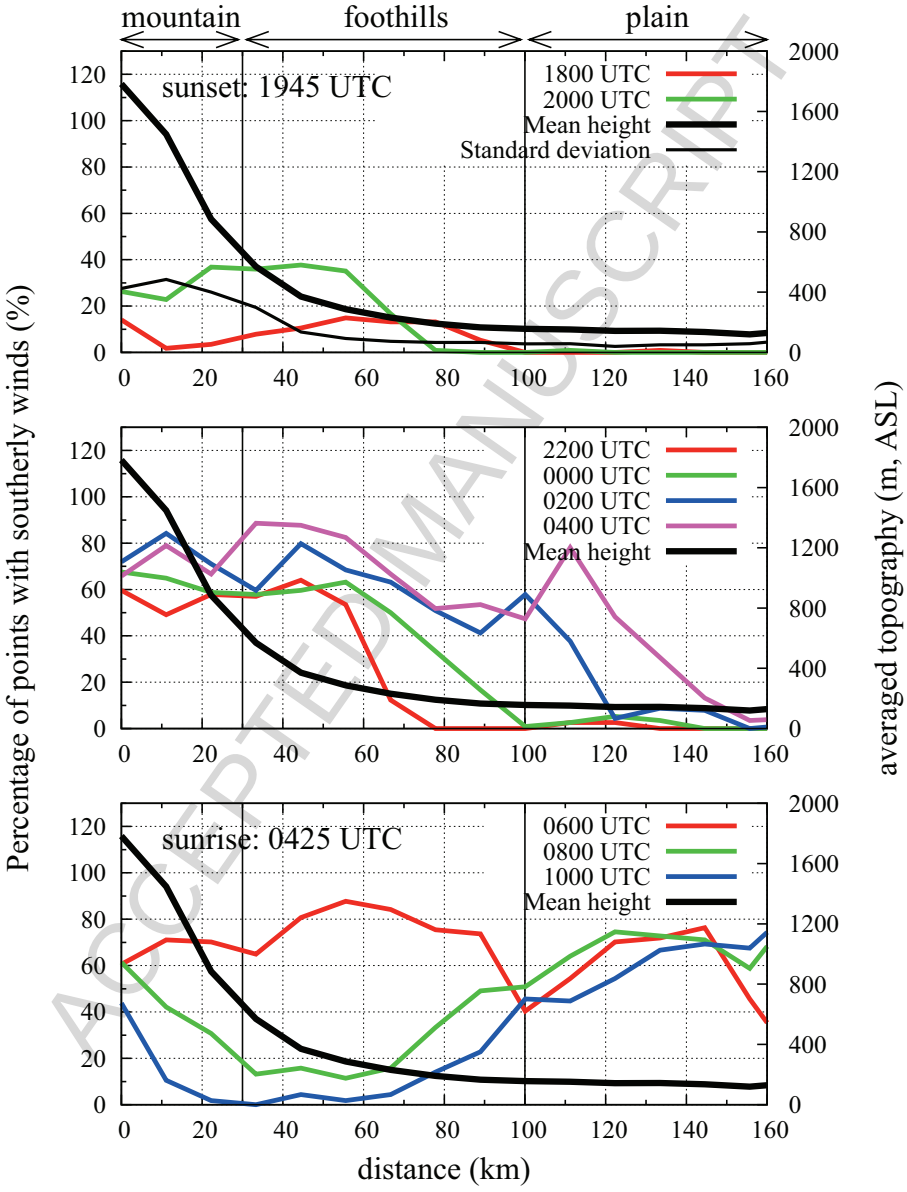

Figure 7: Percentage of the grid points with southerly wind (wind direction below 200 m AGL ranging between 120°-240°) along the black line in Fig. 3 and along an equally long line at a certain distance, perpendicular to it. This percentage is plotted every 2 hours from 1800 UTC to 1000 UTC of the next day. The averaged topography of the whole line (in m, ASL) for each distance from the Pyrenees is shown with a black thick line and the standard deviation with a thinner black line (see right-hand side scale). The vertical lines indicate the three regions with different features explained in the text: mountain, foothills and plain.

from the arrival of the downslope winds generated in the Pyrenees and the Massif Central (see Fig. 3b).

After sunrise (Fig. 7, bottom), the number of points with southerly wind decreases at the foothills (from 90 % to 10 %) and the mountain regions (from 70 % to 30 %, on average), but the latter at a lower rate. This is related to the fact that downslope winds weaken faster than down-valley winds, as it was seen in Fig. 4. However, in the plain this percentage increases up to 0900 UTC (4.5 hours after sunrise). At 1000 UTC in most of the areas in the foothills the wind is from the upslope direction (percentage of southerly wind points close to zero), although the strong and highly channelled down-valley and down-river winds take longer to veer than the downslope winds.

4.2. Temporal and spatial evolution of the maximum wind speed

To further study the downslope and down-valley winds, some statistics are computed for the southerly maximum wind speed points. At every grid point, the wind maximum is inspected up to 350 m AGL and if there are several maximum at different levels, only the lower one is included in the computations. With this restriction the maximum wind speeds are related to downslope or down-valley winds whereas those of another origin are not considered. The following grid points are not included in the statistics: (i) the gridpoints where the wind is weak (close to 1 m s^{-1}) and no significant wind maximum is found, or (ii) the gridpoints that have a wind maximum below 350 m AGL but the wind nose is less than 1 m s^{-1}. It is found that about 50 % of the points in Fig. 7 fulfil these conditions and have a southerly jet at lower levels.

The maximum wind speed and the height of the maximum are averaged over each line (starting from the black line in Fig. 3) in Fig. 8a and 8b, respectively, at some selected instants. The averaged temperature gradient (dT/dz) below the maximum is also computed in Fig. 8c and the wind direction of the maximum at 2200 UTC and 0600 UTC is shown in Fig. 8d as a function of the distance from the Pyrenees.

In the mountain region, the intensity of the averaged wind maximum increases in time since these points are mainly located at the exits of the valleys in the Pyrenees and correspond to valley exit jets. The standard deviation of the averaged wind speed is large in this region (not shown) due to the wind variability, depending if a gridpoint is located at the exit of a valley or not. However, as we move away from the exit of the valleys towards the foothills, the effect of the down-valley winds is reduced and the averaged

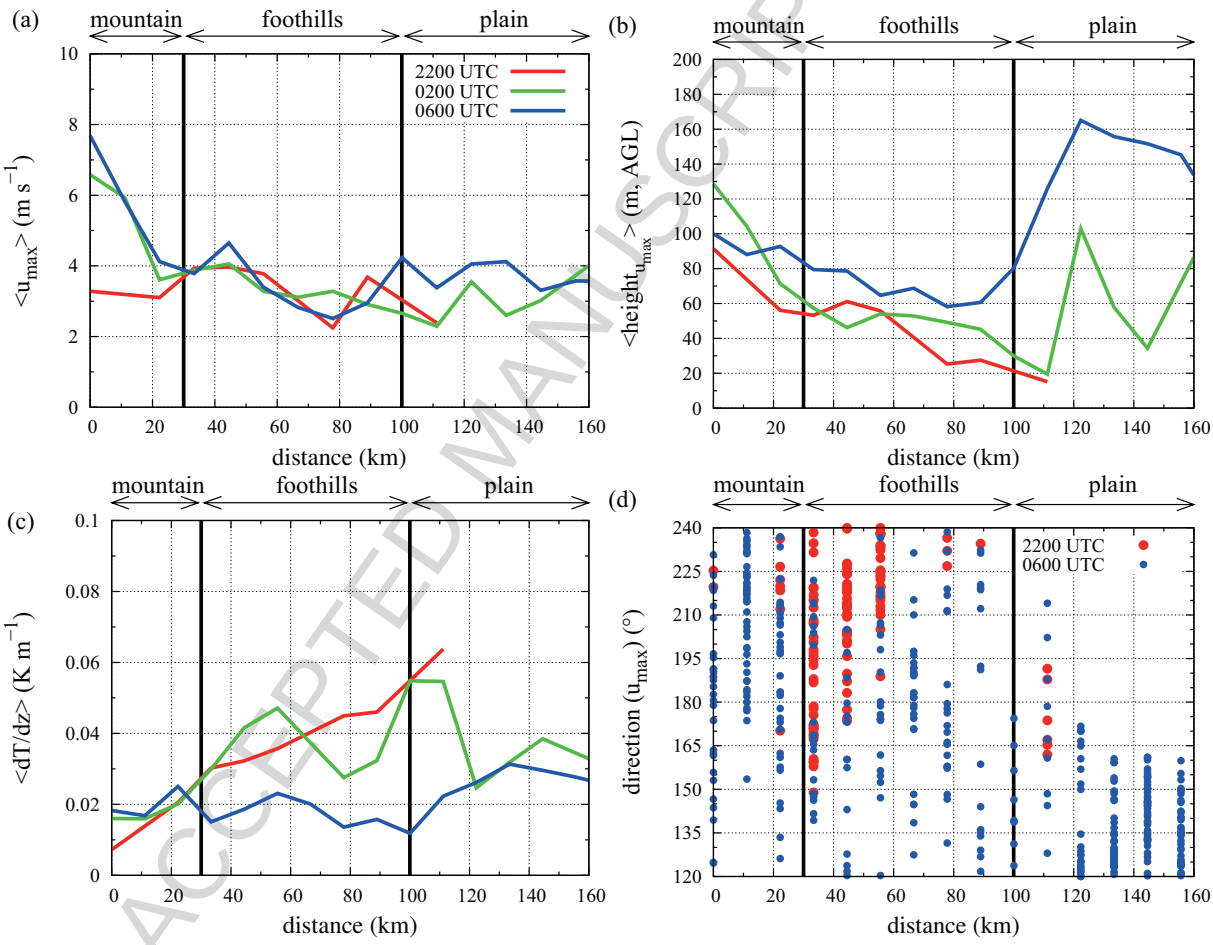

Figure 8: (a) Averaged wind speed (in m s^{-1}) of the southerly wind maxima points for each line (starting from the black line in Fig. 3) as a function of the perpendicular distance from the Pyrenees at three different instants. The same in (b) but for the averaged height (AGL, in m) where the maximum wind is found and in (c) for the averaged temperature gradient below the wind maximum (in K m^{-1}). (d) Direction of the maximum (in °) for the different grid points for a given distance from the Pyrenees at 2200 UTC and 0600 UTC. The vertical black lines indicate the three regions with different features explained in the text: mountain, foothills and plain.

wind maximum and the height where it is found decrease with the distance (Fig. 8a and 8b), as it is seen in Figure 13 in Zhong and Whiteman (2008). The temperature gradient increases as night progresses (Fig. 8c) reaching a stationary state between 0200 and 0600 UTC, when down-valley winds are established (Fig. 8a).

In the foothills region, the intensity of the averaged wind maximum is nearly constant (about 3 m s^{-1}, Fig. 8a). A similar value can be derived from Fig. 7 between 2200 UTC and 0200 UTC (the percentage of points with southerly wind has advanced 40 km in 4 hours towards the plain direction). The downslope winds in this region are located at the same level of the top of the temperature inversion (Fig. 4), a height that slightly decreases with the distance from the Pyrenees (Fig. 8b). In the evening (2200 UTC) the temperature gradient linearly increases with the distance, for the three regions in Fig. 8c. This is related to the fact that near the surface the temperature cools down in the plain faster than in the foothills, in agreement with the satellite observations in Fig. 6. As night progresses, and due to the arrival of downslope winds in the foothills, mixing is produced at lower levels due to the wind shear and the temperature gradient is reduced (Fig. 8c). Since the 2m-temperature decreases when the downslope winds reach a region (for instance in Toulouse, Fig. 2f), when the downslope winds travel through the foothills they are colder than the ambient air, indicating that they behave like a gravity current.

The maximum wind is from south-west at the beginning of the night (2200 UTC, (Fig. 8d), due to the presence of downslope winds (Fig. 3a). However, the values are less focused as the night progresses (Fig. 8d) probably related to the fact that the downslope winds adapt to the local slopes once they reach the foothills region, as in Haiden and Whiteman (2005).

Finally, in the plain region, the progressive accumulation of air in the centre of the river axis makes that the averaged intensity and height of the wind maxima increase as time advances (Fig. 8a and 8b, respectively). The down-river direction is from south-east and nearly constant after midnight (Fig. 8d), in agreement with the observations (Fig. 2b). It is important to mention that the reverse of the wind in this region (from down to up-river) is not completed at the end of the run (1000 UTC) and from the observations in Toulouse it is around 1200 UTC.

5. Conclusions

During calm nights, downslope and down-valley winds are generated at the slopes of the north Pyrenees. From the analysis of the model outputs and the available observations in the foothills region, it is found that downslope winds travel from the mountain to the plain at an average wind speed of 3 m s^{-1} from 2200 UTC to 0400 UTC and they are placed below 100 m above the ground. Once the downslope winds reach a certain location at the foothills, the wind turns towards the downhill direction, the wind speed increases and the 2m-temperature diminishes, indicating that the downslope wind is colder than the ambient air. Thus, the downslope winds behave like a gravity current and the mixing is mainly generated by the wind shear.

Three well defined regions are found to understand the organization of the flow at lower levels:

- *mountain*. At the beginning of the night, downslope winds are generated in the walls of the valleys and favour the accumulation of air in the bottom areas. Thus, down-valley winds are formed, highly channelled, that will from then on be stronger than the downslope flows. As a result, the stronger winds are located at the exits of the valleys, corresponding to valley exit jets, whereas in the rest of the slopes, downslope winds are present. Further work is needed to properly characterise this region. In this work we have focused the attention to the other regions.

- *foothills*. Before sunset, downslope winds appear in the upper foothills and they progress to the lower foothills as night advances with a mean wind speed of 3 m s^{-1}. The time when the turning of the wind (from upslope to downslope) is produced depends on the distance to the Pyrenees, the closer the earlier, in agreement with the observations. The maximum speed of the downslope winds is located at lower levels (below 100 m above the ground) at the temperature inversion height and its intensity remains nearly constant during the night. 1.5 hours after sunrise, the wind starts veering from the downslope to the upslope direction, in agreement with the observations.

- *plain*. Later in the night (around 0200 UTC), the downslope winds from the Pyreness and the Massif Central foothills reach the mid-Garonne region, where down-river winds are formed. The turning of the wind (from uplope to downslope) takes longer in the foothills than in the

plain, in agreement with the observations, since it happens when the downslope winds converge to the river axis. After sunrise (between 0600 UTC and 1000 UTC), the wind direction is from S-SE in the plain. Down-river winds are more difficult to diminish because they are more concentrated and with stronger wind speeds than downslope winds.

At higher levels, it is difficult to find a return current of the downslope winds where the flow can be perturbed by other motions of larger scales (basin or synoptic), specially for complex terrain regions, as the one chosen in this study.

Acknowledgements ECMWF and AEMET are thanked for the access to computing time and the Meso-NH team in Meteo France and Laboratoire d'Aérologie for their support. M. Lothon is acknowledged for providing the climatology study and the observations from Lannemezan. This work was funded through the projects CGL2009-12797-C03-01 and CGL2012-37416-C04-01 of the Spanish Government, supplied by the European Regional Development Fund (FEDER), and with a contract JAE-Doc of the *Junta para la Ampliación de Estudios* program from CSIC supplied by the European Social Fund.

References

Barneoud, P., Beck, S., Lafrique, P., Lagnoux, B., 2010. Climatologie sur le site instrumenté du Laboratoire d'Aérologie. Rapport, Université Paul Sabatier, Toulouse III.

Bastin, S., Drobinski, P., Dabas, A., Delville, P., Reitebuch, O., Werner, C., 2005. Impact of the Rhone and Durance valleys on sea-breeze circulation in the marseille area. Atmos. Res. 74, 303–328.

Belamari, S., 2005. Report on uncertainty estimates of an optimal bulk formulation for surface turbulent fluxes. MERSEA IP Deliverable 412, 1–29.

Bougeault, P., Bénech, B., Bessemoulin, P., Carissimo, B., Jansà, A., Pelon, J., Petitdidier, M., Richard, E., 1997. PYREX: A summary of findings. Bull. Amer. Meteor. Soc. 78, 637–650.

411 Bougeault, P., Jansà, A., Bénech, B., Carissimo, B., Pelon, J., Richard, E.,
412 1990. Momentum budget over the Pyrénées: The PYREX experiment.
413 Bull. Amer. Meteor. Soc. 71, 806–818.

414 Bougeault, P., Lacarrère, P., 1989. Parameterization of orography-induced
415 turbulence in a mesobeta scale model. Mon. Wea. Rev. 117, 1872–1890.

416 Campins, J., Jansà, A., Benech, B., Koffi, E., Bessemoulin, P., 1995. PYREX
417 observation and model diagnosis of the Tramontane wind. Meteorol. At-
418 mos. Phys. 56, 209–228.

419 Cros, B., Durand, P., Cachier, H., Drobinski, P., Frejafon, E., Kottmeier, C.,
420 Perros, P. E., Peuch, V.-H., Ponche, J., Robin, D., Sard, F., Toupance,
421 G., Wortham, H., 2004. The ESCOMPTE program. An overview. Atmos.
422 Res. 69, 241–279.

423 Cuxart, J., Bougeault, P., Redelsperger, J.-L., 2000. A turbulence scheme
424 allowing for mesoscale and large-eddy simulations. Quart. J. Roy. Meteor.
425 Soc. 126, 1–30.

426 Cuxart, J., Holtslag, A. A. M., Beare, R. J., Bazile, E., Beljaars, A., Co-
427 nangla, L., Ek, M., Freedman, F., Hamdi, R., Kerstein, A., Kitagawa,
428 A., Lenderink, G., Lewellen, D., Mailhot, J., Mauritsen, T., Perov, V.,
429 Schayes, G., Steeneveld, G.-J., Svensson, G., Taylor, P., Weng, W., Wun-
430 sch, S., Xu, K.-M., 2006. Single-column model intercomparison for a stably
431 stratified atmospheric boundary layer. Bound.-Layer Meteor. 118, 273–303.

432 Cuxart, J., Jiménez, M. A., 2012. Deep radiation fog in a wide closed valley:
433 Study by numerical modeling and remote sensing. Pure Appl. Geophys.
434 169, 911–926.

435 Cuxart, J., Jiménez, M. A., Martínez, D., 2007. Nocturnal meso-beta basin
436 and katabatic flows on a midlatitude island. Mon. Wea. Rev. 135, 918–932.

437 Cuxart, J., Jiménez, M. A., Martínez, D., Molinos, F., Cunillera, J., Palau,
438 J.-L., 2012. Study of mesobeta basin flows by remote sensing. Bound.-Layer
439 Meteor. 143, 143–148.

440 Durran, D. R., 1989. Improving the anelastic approximation. J. Atmos. Sci.
441 46, 1453–1461.

Edwards, J. M., 2009. Simulation of land surface temperatures: comparison of two climate models and satellite retrievals. Geosci. Model Dev. 2, 123–136.

Fouquart, Y., Bonnel, B., 1980. Computations of solar heating of the Earths Atmosphere: A new parametrization. Beitr. Phys. Atmosph. 53, 35–62.

Haiden, T., Whiteman, C. D., 2005. Katabatic flow mechanisms on a low-angle slope. J. Appl. Meteor. 44, 113–126.

Jiménez, M. A., Cuxart, J., 2005. Large-Eddy Simulations of the stable boundary layer using the standard Kolmogorov theory: Range of applicability. Bound.-Layer Meteor. 115, 241–261.

Jiménez, M. A., Mira, A., Cuxart, J., Luque, A., Alonso, S., Guijarro, J.-A., 2008. Verification of a clear-sky mesoscale simulation using satellite-derived surface temperatures. Mon. Wea. Rev. 136, 5148–5161.

Lafore, J. P., Stein, J., Asencio, N., Bougeault, P., Ducrocq, V., Duron, J., Fisher, C., Héreil, P., Mascart, P., Pinty, J.-P., Redelsperger, J.-L., Richard, E., de Arellano, J. V.-G., 1998. The Meso-NH atmospheric simulation system. Part I: Adiabatic formulation and control simulation. Ann. Geophys. 16, 90–109.

Laiti, L., Zardi, D., Franceschi, M., Rampanelli, G., 2013. Atmospheric boundary layer structures associated with the Ora del Garda wind in the Alps as revealed from airborne and surface measurements. Atmos. Res. 132-133, 473–489.

Lothon, M., Lenschow, D.-H., Angevine, W., Bange, J., Beare, B., Canut, G., Couvreux, F., Delbarre, H., Durrand, P., Gibert, F., Gioli, B., Jonker, H., Lohou, F., Mahrt, L., Pardyjak, E., Pino, D., de Arellano, J. V.-G., 2010. Studying the Boundary Layer Late Afternoon and Sunset Turbulence (BLLAST). 15th International Symposium for the Advancement of Boundary Layer Remote Sensing (ISARS 2010), 1–4.

Martínez, D., Cuxart, J., 2009. Assessment of the hydraulic slope flow approach using a mesoscale model. Acta Geophys. 57, 882–903.

Martínez, D., Jiménez, M. A., Cuxart, J., Mahrt, L., 2010. Heterogeneous nocturnal cooling in a large basin under very stable conditions. Bound.-Layer Meteor. 137, 97–113.

Masson, V., 2000. A physically-based scheme for the urban energy budget in atmospheric models. Bound.-Layer Meteor. 94, 357–397.

Masson, V., Bougeault, P., 1996. Numerical simulation of a low-level wind created by complex orography: A Cierzo case study. Mon. Wea. Rev. 124, 701–715.

Masson, V., Champeaux, J.-L., Chauvin, C., Meriguet, C., Lacaze, R., 2003. A global database of land surface parameters at 1 km resolution for use in meteorological and climate models. J. Climate 16, 1261–1282.

Mlawer, E. J., Taubman, S. J., Brown, P. D., Iacono, M. J., Clough, S. A., 1997. Radiative transfer for inhomogeneous atmospheres: RRTM. A validated correlated-k model for the longwave. J. Geophys. Res. 102, 16663–16682.

Morcrette, J.-J., 1990. Impact of changes to the radiation transfer parameterizations plus cloud optical properties in the ECMWF model. Mon. Wea. Rev. 118, 847–873.

Noilhan, J., Planton, S., 1989. A simple parameterization of land surface processes for meteorological models. Mon. Wea. Rev. 117, 536–549.

Pamperin, H., Stilke, G., 1985. Nocturnal boundary layer and low level jet near the Inn valley exit. Meteor. Rundsch. 38, 145–156.

Salomonson, V. V., Bames, W. L., Montgomery, W. P., Ostrow, H., 1989. MODIS: advanced facility instrument for studies of the Earth as a system. IEEE Trans. Geosci. Remote Sens. 27, 145–153.

Seaman, N. L., Gaudet, B. J., Stauffer, D. R., Mahrt, L., Richardson, S. J., Zielonka, J. R., Wyngaard, J. C., 2012. Numerical prediction of submesoscale flow in the nocturnal stable boundary layer over complex terrain. Mon. Wea. Rev. 140, 956–977.

Warner, T. T., Peterson, R. A., Treadon, R. E., 1997. A tutorial on lateral boundar conditions as a basic and potentially serious limitation to regional numerical weather prediction. Bull. Amer. Meteor. Soc. 78, 2599–2617.

Whiteman, C. D., 2000. Mountain meteorology. Fundamentals and applications. Oxford University Press.

Zhang, Y., Duliere, V., Mote, P. W., Salathe, E. P., 2009. Evaluation of WRF and HadRM Mesoscale Climate Simulations over the U.S]. Pacific Northwest. J. Climate 22, 5511–5526.

Zhong, S., Whiteman, C. D., 2008. Downslope flows in a low-angle slope and their interactions with valley inversions. Part II: Numerical modeling. J. Appl. Meteor. Climatol. 47, 2039–2057.

Highlights

1) The organization of the mountain-valley flow at lower levels during the night-time and under clear-skies and weak wind conditions is presented here.
2) The foothills of the north Pyrenees are selected to study the temporal and spatial scales of the downslope winds through a high-resolution mesoscale simulation.
3) At the Pyrenees foothills, the turning of the wind (from upslope to downslope) starts before sunset but it depends on the distance to the Pyrenees, the closer the earlier.
4) A statistical analysis of the model outputs is made to find the temporal and spatial scales of the downslope winds.